American Mineralogist, Volume 88, pages 121–130, 2003

Correction of secondary X-ray fluorescence near grain boundaries in electron microprobe analysis: Application to thermobarometry of spinel lherzolites

XAVIER LLOVET[1,*] AND GUMER GALAN[2]

[1]Serveis Cientificotècnics, Universitat de Barcelona. Lluís Solé i Sabarís, 1-3. 08028 Barcelona, Spain
[2]Departament de Geologia, Universitat Autónoma de Barcelona. Edifici C (S). 08193 Bellaterra, Barcelona, Spain

ABSTRACT

A correction procedure is proposed to account for the effect of secondary X-ray fluorescence near grain boundaries in electron microprobe analysis. The procedure is based on the Monte Carlo simulation method, which is used to calculate the X-ray spectrum emitted by the mineral couple (i.e., the mineral of interest with the neighboring mineral). The contribution of secondary fluorescence from the neighboring mineral, which appears in the simulated spectrum in a natural way, is then subtracted from the measured *k*-ratio and thereafter conventional matrix corrections are applied. The Monte Carlo simulation algorithm used is largely based on the general-purpose simulation package PENELOPE. In order to assess the reliability of this code, simulated "apparent" element profiles are compared with electron microprobe measurements found in the literature, in which the effect of secondary fluorescence was characterized and the reliability of the different assumptions underlying the proposed procedure is discussed.

Finally, the procedure is used to assess data from the olivine-clinopyroxene thermobarometer in a spinel lherzolite xenolith. The application of the secondary fluorescence correction leads to: (1) higher systematic pressure estimations than those obtained from uncorrected data, with lower uncertainties; and (2) a better agreement between the olivine-clinopyroxene temperature estimations and those estimated using the two-pyroxene thermometer. Estimated *P-T* conditions indicate a decompressional path with a slight decrease in temperature from core to crystal rim. However, if the effect of secondary fluorescence is not taken into account, an apparent heating event is observed.

INTRODUCTION

Electron microprobe analysis (EMPA) is a reliable, nondestructive technique for the quantitative analysis of rock-forming minerals (see e.g., Reed 1993). The technique is based on the measurement of characteristic X-ray intensities emitted by the elements that make up the mineral when it is bombarded with a focused electron beam. For each element, the ratio of the X-ray intensity emitted from an unknown to that emitted from a standard of known composition, measured under the same analytical conditions is, to a first approximation, proportional to the ratio of elemental concentrations. A more accurate value of the concentration is obtained by correcting for the differences in electron and photon transport between the unknown mineral and the standard, using the so-called "matrix correction" procedures.

Matrix correction procedures usually assume that the analyzed sample region from which X-rays are emitted has a homogeneous composition. The volume of this region can be estimated by calculating the effective penetration range of incident electrons. For keV electron beams, this range is typically of the order of several micrometers, depending on the material and the analytical conditions. Accordingly, EMPA is adequate for analyzing homogeneous mineral grains that have a diameter larger than several micrometers. However, the range of characteristic X-rays and Bremsstrahlung that are generated by incident electrons, is typically one to two orders-of-magnitude greater, namely several tens or hundreds of micrometers. Consequently, although the electron beam impacts quite a distance from the grain boundary, X-rays may reach a neighboring phase and induce further ionizations (if the photon energy is larger than the binding energy of the considered atomic shell) causing the emission of characteristic X-rays, and this process is usually referred to as secondary fluorescence (SF). As matrix corrections assume chemical homogeneity, the contribution of SF coming from the adjacent mineral will not be taken into account and will lead to an erroneous concentration. Fortunately, this effect is generally small and it can be disregarded. However, in certain situations, SF coming from a neighboring phase should be taken into consideration carefully. One such situation is the analysis for a minor or trace element in a mineral that coexists with another mineral containing the element of interest. In this case, even if we analyze the mineral relatively far from the boundary, SF may affect the results not only qualitatively but also quantitatively. Examples of interest in geology include the analysis for Ti in chromite in contact with ilmenite (Maaskant and Kaper 1991), Ca in olivine close to clinopyroxene (Dalton and Lane 1996), or Ti in garnet close to rutile or ilmenite inclusions (Feenstra and Engi 1998).

The contribution of SF can be minimized by using *L*-lines instead of *K*-lines in the quantitative procedure (Pouchou 1996).

* E-mail: xavier@giga.sct.ub.es

However, measurement and quantification using *L*-lines is difficult and may lead to larger uncertainties. Besides, for some elements such as Ca, the use of the *L*-line is not a realistic alternative. Several methods have been proposed for correcting SF near phase boundaries (see Dalton and Lane 1996 and references therein). For example, Bastin et al. (1983) developed a numerical method to correct for SF effects in metal couples that can be incorporated into a matrix correction procedure. Myklebust and Newbury (1994) used the Monte Carlo (MC) simulation of electron transport in metal couples to predict SF induced at phase boundaries. These numerical corrections were applied mainly to single-element materials and, moreover, SF induced by the continuum was approximated by very crude methods or even neglected.

In this work, a new correction method is proposed to account for the effect of SF near phase boundaries. The method is based on the simulation of the full X-ray spectrum emitted by the mineral couple, using the MC simulation method. The MC algorithm used is the one developed by Acosta et al. (1998), which is based on a modified version of the general-purpose simulation package PENELOPE (Baró et al. 1995). This code allows the simulation of coupled electron-photon transport in complex material structures consisting of homogeneous regions of arbitrary composition, limited by quadric surfaces. Because both electron and photon transport is considered, the contribution of SF appears in the X-ray spectrum in a natural way and also includes the continuum contribution. In this work, minerals are assumed to be separated by a planar interface; however PENELOPE allows the simulation of other geometries, such as inclined or curved boundaries (Llovet et al. 2000). To assess the reliability of this MC algorithm, simulated element profiles are compared with the EMPA measurements of Dalton and Lane (1996). Those measurements consisted of apparent Ca profiles, which are the result of the effect of SF near grain boundaries, obtained from mineral couples of olivine of increasing Fe content with diopside, and from San Carlos olivine with minerals of increasing Ca content. As an application, we address the problem of analyzing Ca in olivine close to clinopyroxene in spinel lherzolites for purposes of thermobarometry. Indeed, olivine can contain a large amount of Fe and thus emitted Fe$K\alpha$ X-rays can be absorbed in coexisting clinopyroxene by Ca atoms, with the result of the emission of secondary Ca$K\alpha$ X-rays. This contribution is not negligible, as the Ca content in olivine is typically below 1 wt%. Using conventional EMPA correction procedures, the Ca content in olivine was always found to depend on the distance of the electron beam point of impact from the olivine border: the closer the point, the higher the Ca concentration (Adams and Bishop 1986; Jurewicz and Watson 1988; Kölher and Brey 1990; Dalton and Lane 1996). To avoid such contamination prudently, the latter authors recommended that olivine crystals should be physically separated, mounted on a Ca-free matrix, and analyzed separately. The aim of the present study is to provide an alternative method in an attempt to avoid the physical separation of crystals, which is always tedious and sometimes difficult, e.g., when the phase of interest encloses the contaminant mineral as an inclusion (cf., Feenstra and Engi 1998).

MONTE CARLO SIMULATION OF SECONDARY X-RAY FLUORESCENCE

The penetration and slowing down of a particle (electron or photon) in matter is the result of a sequence of interactions in which the particle is deflected and loses energy. Due to the random nature of these interactions, the Monte Carlo (MC) method is particularly well suited for the numerical simulation of particle trajectories within the material medium. Each trajectory is viewed as a sequence of free flights that end with a scattering event where the particle changes its direction, loses energy, and may generate secondary particles. The trajectory finishes when the particle is stopped in the material or escapes from it. Quantities of interest are obtained by averaging over a great number of simulated trajectories. The usefulness of MC simulation stems from its ability to incorporate realistic physical interation models for the scattering mechanisms, and to keep track of the evolution of all particles (secondary electrons, Auger electrons, characteristic X-rays, Bremsstrahlung photons) generated by primary electrons and their descendents.

In the keV range, the possible interactions of electrons with matter are elastic interactions, inelastic collisions, and Bremsstrahlung emission. Elastic interactions change the direction of the electron. Inelastic interactions are those in which the target is brought to an excited state, i.e., a part of the electron's kinetic energy is taken up by the atomic electrons. Inelastic interactions with relatively large energy transfer normally cause the ionization of the target atom. Excited ions relax to their ground state by migration of the initial vacancy to outer electron shells, which proceeds through emission of primary X-rays or Auger electrons with characteristic energies. Emission of Bremsstrahlung takes place when the electron is decelerated within the electrostatic field of the target atom.

Emitted photons (either as characteristic X-rays or Bremsstrahlung) can further interact with the target via photoelectric absorption, Compton scattering, and Rayleigh scattering. In the case of photoelectric absorption, the photon is absorbed and an atomic electron is ejected from the target atom. The resulting ion relaxes by migration of the vacancy to outer electrons shells, with the emission of (secondary) fluorescent X-rays or Auger electrons.

To calculate the SF contribution, we have simulated X-ray spectra using the MC simulation program of Acosta et al. (1998). This program calls a modified version of the PENELOPE subroutine package (Baró et al. 1995) and provides the X-ray spectrum for a given take-off angle. PENELOPE is a general-purpose simulation package that generates electron-photon showers in homogeneous media of arbitrary composition, for a wide energy range, from about 1 keV up to about 1 GeV. The interaction models implemented in PENELOPE are based on the most reliable information available. They combine results from first-principles calculations (this is the case, for example, for electron elastic scattering or photon Compton scattering), semi-empirical models (in electron inelastic scattering), and information from evaluated databases. The scattering models implemented in the code, together with the simulation algorithm, have been described in detail elsewhere (Baró et al. 1995; Sempau et al. 1997). PENELOPE also includes a package for simulation of complex geometries con-

sisting of homogeneous bodies limited by quadric surfaces. The complete code system (FORTRAN source files and database) is available from the NEA[1] data bank.

VALIDATION OF THE MONTE CARLO SIMULATION ALGORITHM

The reliability of MC simulation largely depends on the accuracy of the underlying scattering model adopted to describe the interactions of electrons and photons with matter. Therefore, it is important to assess the adequacy of a MC code to the particular application of interest.

Recently, it was shown that the MC algorithm of Acosta et al. (1998) correctly reproduces "apparent" *k*-ratio profiles in selected metal couples near phase boundaries (Valovirta et al. 2001). For example, Figure 1 illustrates simulated and measured *k*-ratio profiles for an Fe-Cu couple as a function of the distance from the electron beam to the interface. The Fe *k*-ratio in Cu (right side of Fig. 1) is caused by fluorescence from the continuum and the characteristic Cu X-rays absorbed in the Fe region, whereas the apparent Cu *k*-ratio in Fe results from fluorescence from the Fe continuum in Cu. The agreement between simulation results and measurements is fully satisfactory.

To assess further the accuracy of the MC algorithm used in this work, the EMPA measurements of Dalton and Lane (1996) were simulated. These measurements consist of "apparent" Ca profiles in olivine, as a function of the distance from the point of impact of the electron beam to the boundary, from couples consisting of olivine grains (having an increasing Fe content) with diopside, and couples of San Carlos olivine with minerals with an increasing Ca content. To calculate each theoretical spectrum, we simulated 500 000 primary electron tracks. Relative uncertainties of the simulated Ca profiles range from 8–15%. Figure 2 compares simulated and experimental apparent Ca profiles in olivine ($Fo_{99.5}$, $Fo_{90.7}$, Fo_{30}, and $Fo_{8.4}$) couples with diopside, and in San Carlos olivine ($Fo_{90.7}$) with bytownite and calcite. We can see that SF increases as analyses are taken closer to the boundary. In all the analyzed cases, the experimental data of Dalton and Lane (1996) were found to agree satisfactorily with our MC simulations.

[1]OECD Nuclear Energy Agency Data Bank. Le Seine Saint-Germain, 12. Boulevard des Iles, 92130 Issy-les-Moulineaux, France (E-mail: nea@nea.fr).

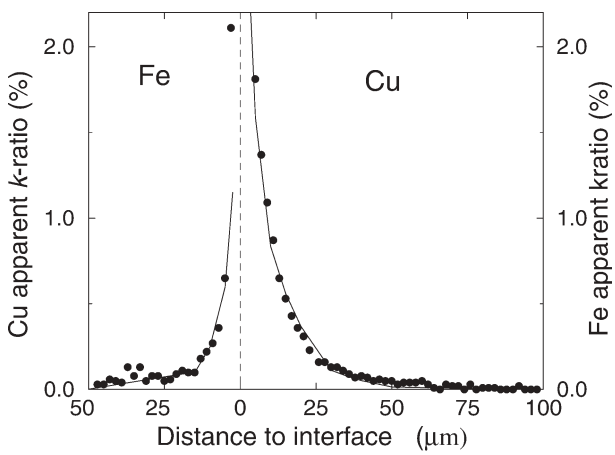

FIGURE 1. Apparent Cu and Fe *k*-ratio profiles from secondary fluorescence for an Fe-Cu couple vs. distance to interface. The Fe *k*-ratio in Cu (right-hand side of the figure) is caused by fluorescence from the continuum and the Cu$K\alpha$ X-rays absorbed in the Fe region, while the apparent Cu *k*-ratio in Fe results from fluorescence from the Fe continuum in Cu. Solid lines represent results of Monte Carlo simulations. Filled circles are measurements from Valovirta et al. (2001).

SECONDARY FLUORESCENCE CORRECTION

The secondary fluorescence correction is performed in several steps. In the first step, we analyze the mineral under consideration and the contaminant mineral with the electron microprobe. The mineral compositions furnish the input data file of the simulation program, which is run in batch mode to obtain X-ray spectra for electron beams impacting along a line perpendicular to the interface, from the interface up to a distance 100 micrometers away. In the simulations, we assume that minerals are separated by a planar interface. We also assume that the element of interest is not present in the mineral under electron bombardement. This approximation is plausible for trace elements as they do not substantially modify the stopping power of the mineral; however, this assumption makes our procedure unsuitable for the correction of other major elements.

To avoid background subtraction of simulated spectra, Bremsstrahlung photons are not counted when escaping from the surface, unless they have interacted in the medium. Therefore, although the generation and transport of Bremsstrahlung photons is simulated, X-ray emission spectra consist only of X-ray peaks, and extracting their intensities is straightforward. When each simulation is complete, we store the *k*-ratio of the element of interest and the distance of the electron beam to the boundary in a separate file. Linear interpolation is then used to calculate the *k*-ratio at the distance actually measured by EMPA, which is estimated from the measured profile along a line crossing the interface. The interpolated *k*-ratio is then subtracted from the measured *k*-ratio and matrix corrections are applied. In the simulations of Ca *k*-ratios in olivine done in this study, the relative statistical uncertainties range typically from 5–20% (2σ level).

APPLICATION TO THERMOBAROMETRY OF SPINEL LHERZOLITES

In an attempt to validate further the SF correction close to phase boundaries, we have analyzed olivine crystals in contact with clinopyroxene to estimate the *P-T* path of an ultramafic xenolith entrained by the mafic alkaline pyroclasts of the Canet d'Adri volcano (Girona, Catalonia, NE Spain). The uncertainty and deviation of corrected and uncorrected results are compared and the effect on the geological history is assessed.

Catalan mafic alkaline volcanism is Neogene-Quaternary in age and is characterized by the extrusion of basanites, leucite basanites, and alkali basalts, with minor trachytes (Tournon 1968; Araña et al. 1983; López Ruiz and Rodríguez Badiola 1985; Cebriá et al. 2000). This volcanism has been related to middle-late Alpine extensional fractures (Araña et al. 1983; Martí et al. 1992), as is the case in the central-western Euro-

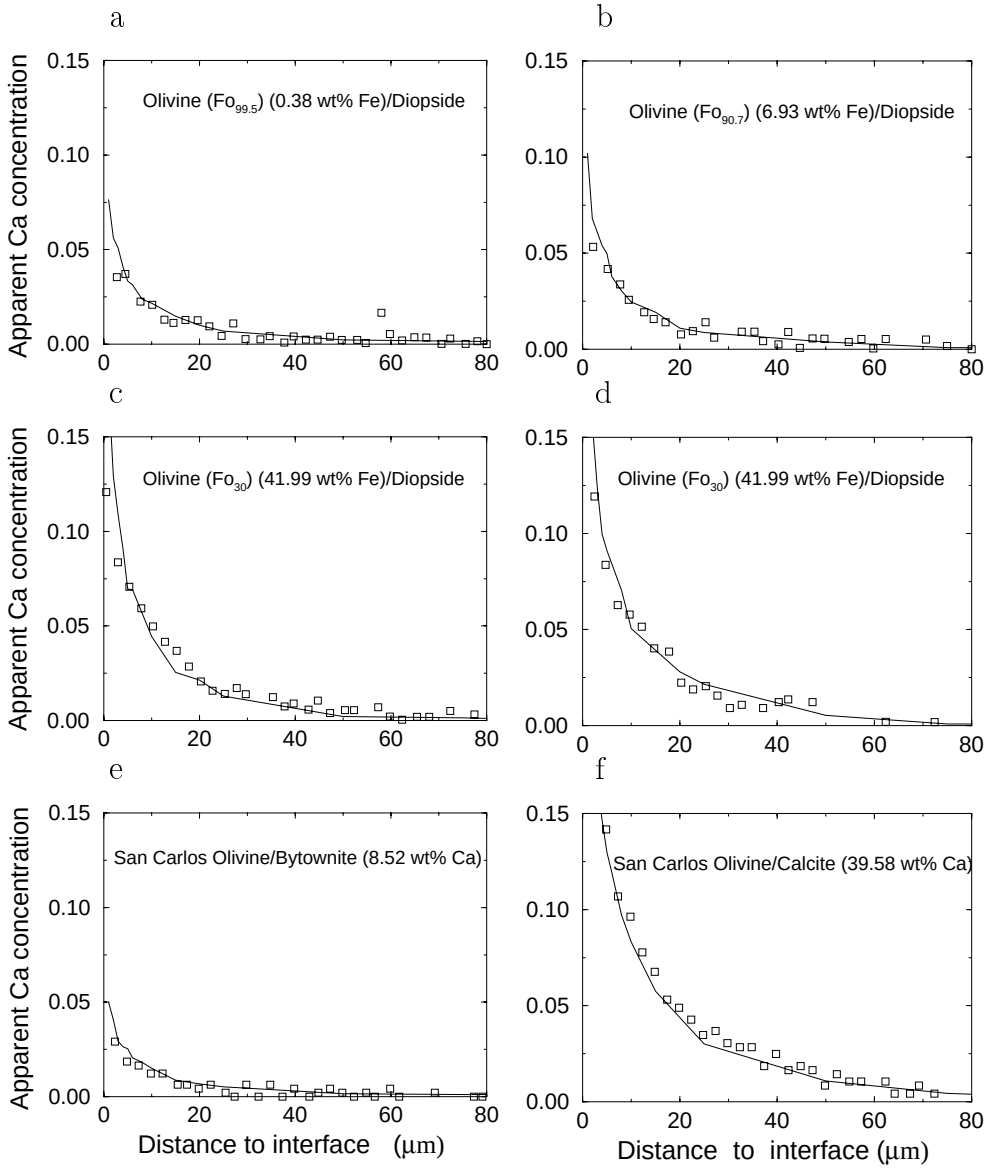

FIGURE 2. (a–f) Apparent Ca concentration profiles from secondary fluorescence vs. distance to interface in olivine from different olivine couples with other minerals, as indicated in the legends. Lines represent results of Monte Carlo simulations. Open symbols are measurements from Dalton and Lane (1996).

pean volcanic province where similar lavas are widespread (Wilson and Downes 1990). The presence of ultramafic xenoliths in some of the pyroclastic deposits and lava flows of the area was first noted by Tournon (1968), who provided a detailed petrologic description of them. He distinguished two main types of ultramafic xenoliths: (1) peridotite xenoliths, and (2) pyroxenites, hornblendites, and gabbro xenoliths. The sample studied (CA.00.83) belongs to the first type and is 5 cm in size (Fig. 3a). It is a protogranular, medium-grained (diameter <5 mm) spinel lherzolite with 65% olivine, 21% orthopyroxene, 13% clinopyroxene, and 1% spinel (modal amounts), similar to typical protogranular mantle xenoliths found in alkali basalts (see Nixon 1987 and references therein).

Analytical methods

Analyses were performed on a CAMECA SX-50 electron microprobe, at the Serveis Cientificotècnics of the University of Barcelona, with an accelerating voltage of 20 kV and a beam current of 15 nA. To minimize statistical uncertainties within reasonable counting times, Ca was analyzed separately with a beam current of 100 nA. Counting times ranged between 10 and 30 sec. Analyzing crystals were TAP, PET, and LiF. Calibration was performed using silicate and oxide standards. Raw intensity data were corrected for dead time and spectral background. *K*-ratios were corrected for matrix effects using the method of Pouchou and Pichoir (1984), which is implemented in the microprobe software. The detection limit for Ca in oliv-

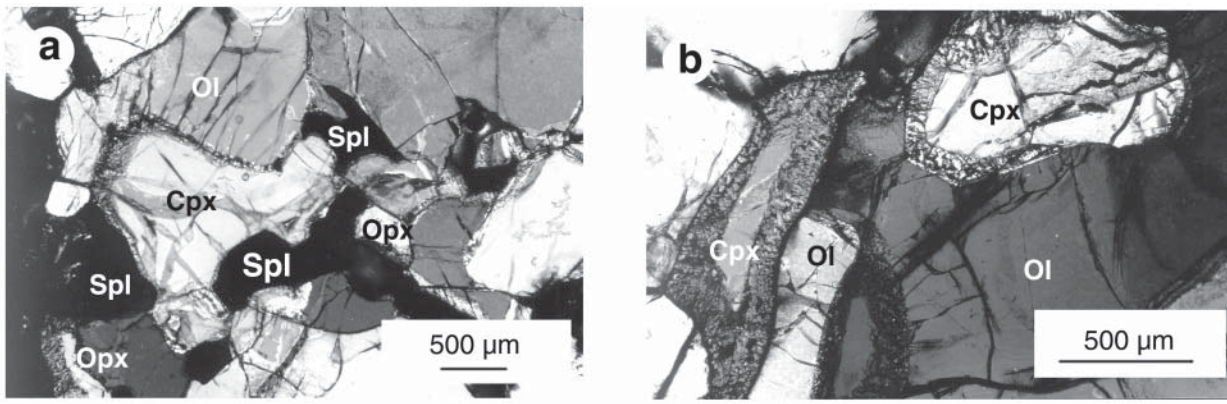

FIGURE 3. (**a**) Characteristic protogranular texture of sample CA.00.83. A cluster of spinel and pyroxene crystals is present. (**b**) Clinopyroxene crystals with dendritic rims adjoining olivine. Mineral abbreviations after Kretz (1983).

ine (at the 2σ confidence level) is 0.007 wt% and the relative error is about 5% for 0.15 wt% Ca and 10% for 0.08 wt% Ca.

When attempting to correct for SF effects near grain boundaries using a wavelength-dispersive spectrometer (WDS), one finds a further analytical uncertainty, namely the intensity loss due to crystal defocusing of X-rays emitted far from the electron beam point of impact, such as SF X-rays emitted from a neighboring mineral (Dalton and Lane 1996). As a consequence, SF intensity will depend on the orientation of the sample with respect to the spectrometer. To minimize this effect, line profiles were always oriented, as much as possible, in the direction toward the spectrometer. Along this direction, the effect of crystal defocusing was estimated to be less than 5% up to about 50 micrometers farther from the point of impact of the electron beam.

Mineral chemistry

Olivine crystals are xenomorphic with deformation bands and subgrains. Their composition is $Fo_{92–89}$ (Table 1) and zoning is typically absent, but a slight decrease in Fo (ca. 1%) from the core to the rim is present in some crystals. No systematic variation was observed in NiO concentration (0.47–0.12 wt%), however, CaO concentration is systematically higher toward the rim (from 0.11 up to 0.47 wt%) if the effect of Ca contamination from adjoining clinopyroxene by the SF effect is not corrected. This correction is crucial because accurate measurement of Ca in olivine coexisting with clinopy-roxene is essential for estimating the equilibrium pressure of these rocks; the Ca exchange reaction between olivine and clinopyroxene (Köhler and Brey 1990) is the only barometer that can be applied successfully to spinel peridotites. In our case, SF effects near phase boundaries can be avoided either by physically separating the olivine crystals or by targeting the olivine at a distance greater than, say, 50 µm from the interface owing to the fact that olivine crystals are several millimeters in diameter. However, a knowledge of entire Ca profiles is useful for estimating the earlier *P-T* conditions and later thermal evolution of the xenolith, before and while it became entrained in the host lava. Although physical separation of olivine crystals was proven to be successful in dealing with the SF problem (Köhler and Brey 1990; Dalton and Lane 1996; Werling and Alther 1997), it is always tedious. Moreover, unless the whole sample is at equilibrium, it would be difficult to select which clinopyroxene crystal was actually in contact with the separated olivine crystal, and could result in losing some important information on local re-equilibrium of minerals. These drawbacks can be overcome by the application of the proposed SF correction.

Clinopyroxene crystals are xenomorphic. Some of them show clean, sharp contacts with other minerals, but most have dendritic rims, up to 100 micrometers wide, which are the result of their being partially melted (Fig. 3b). Compositional mapping of these dendritic crystals indicates that the dendrites are filled with Al- and Na-enriched glass relative to clinopyroxene. Figure 4 illustrates a compositional profile across one of these crystals that becomes irregularly depleted in Al and Na, whereas both Ca and Mg increase at the dendritic rim, as is the case of Mg no. [Mg no. = 100 Mg/(Mg + Fe^{2+}); cations per formula unit]. This compositional variation is similar to that observed in clinopyroxene crystals from spinel lherzolites that were heated experimentally or naturally (Tsuchiyama 1986; Doukhan et al. 1993; Shaw and Edgar 1997). Representative analyses of clinopyroxene are included in Table 1. The formula unit and Fe^{3+} were calculated on the basis of four cations following the method of Robinson (1982). The clinopyroxenes are chromian and aluminian, and Figure 5 indicates that their compositions are Mg-rich augite and diopside (Morimoto et al. 1988). The former composition corresponds to the crystal cores, whereas the latter is typical of the dendritic rims. Mg no. is slightly higher than in olivine, but it is more similar when Fe_{total} is considered as Fe^{2+}.

Orthopyroxene is also rich in Al and Cr (chromian aluminian enstatite; Morimoto et al. 1988), with Mg no. similar to %Fo in olivine (Fig. 5), and slightly lower than in clinopyroxene. Representative analyses are also included in Table 1. No systematic zoning was observed.

Spinel forms xenomorphic crystals that enclose pyroxenes. Spinel and pyroxene form clusters (Fig. 3a) that were interpreted as the phases resulting from the reaction olivine + garnet = spinel + pyroxenes (Witt-Eickschen 1993; Witt-Eickschen

TABLE 1. Representative analyses of olivine, pyroxenes and spinel. Non corrected CaO concentration in olivine for SF is represented in brackets

SAMPLE	CA.00.83									
%Oxides	Ol 49c	Ol 6r	Cpx 55c	Cpx 52r	Cpx 41dr	Opx 56	Opx46	%Oxides	Spl 2c	Spl 3r
SiO_2	40.48	40.14	52.15	51.29	51.35	54.05	54.83	SiO2	0.12	0.14
Al_2O_3	0.04	0.03	6.79	6.84	5.43	5.34	5.44	TiO2	0.25	0.20
TiO2	0.00	0.04	0.36	0.38	0.45	0.12	0.13	Al_2O_3	51.59	51.14
Cr_2O_3	0.07	0.03	1.03	1.02	1.26	0.55	0.57	Cr_2O_3	13.87	13.95
FeO	9.78	9.46	3.74	3.77	3.34	6.21	6.04	Fe_2O_3	4.38	4.32
MnO	0.08	0.12	0.04	0.15	0.07	0.14	0.13	FeO	8.84	8.32
MgO	49.24	49.28	16.60	16.43	16.94	32.24	32.30	MnO	0.10	0.10
NiO	0.40	0.36	0.05	0.03	0.03	0.10	0.11	MgO	20.07	20.12
CaO	[0.12]0.12	[0.18]0.13	18.27	17.96	20.90	1.19	1.15	NiO	0.36	0.42
Na_2O			1.43	1.52	0.39	0.16	0.14			
Total	100.09	99.46	100.46	99.39	100.16	100.10	100.84	Total	99.58	98.71
	O = 4		cations = 4						O = 32	
Si	0.992	0.989	1.870	1.858	1.861	1.865	1.880	Si	0.025	0.029
IVAl	0.001	0.001	0.130	0.142	0.139	0.135	0.120	Ti	0.040	0.033
VIAl			0.157	0.150	0.093	0.082	0.100	Al	12.890	12.870
Ti	0.000	0.001	0.010	0.010	0.012	0.003	0.003	Cr	2.326	2.355
Cr	0.001	0.001	0.029	0.029	0.036	0.015	0.016	Fe^{3+}	0.699	0.695
Fe^{3+}			0.023	0.049	0.014	0.042	0.008	Fe^{2+}	1.568	1.486
Fe^{2+}	0.200	0.195	0.090	0.065	0.087	0.138	0.165	Mn	0.017	0.018
Mn	0.002	0.003	0.001	0.005	0.002	0.004	0.004	Mg	6.345	6.406
Mg	1.799	1.810	0.887	0.887	0.915	1.658	1.651	Ni	0.061	0.072
Ni	0.008	0.007	0.001	0.001	0.001	0.003	0.003			
Ca	0.003	0.003	0.702	0.697	0.812	0.044	0.042			
Na			0.099	0.107	0.028	0.011	0.009			
%Fo	89.98	90.28								
%Wo			41.22	40.93	44.37	2.33	2.25			
%En			52.08	52.08	50.00	87.91	88.29			
%Fs			6.69	6.99	5.63	9.76	9.47	cations	23.971	23.964
Mg no.			90.79	93.17	91.32	92.32	90.91	Mg no.	80.18	81.17
Cr no.			9.18	9.03	13.43	6.47	6.78	Cr no.	15.29	15.47
T			2.000	2.000	2.000	2.000	2.000			
M1			1.000	1.000	1.000	1.000	1.000			
M2			0.999	1.000	1.000	1.000	1.001			

Notes: c = core; r = rim; dr = dendritic rim. Mg no. = 100.Mg/(Mg+Fe^{2+}). Cr no. = 100.Cr/(Cr+Al).

and Kramm 1997). The spinel compositions are pleonaste (Table 1), with Mg no. = 84–80 and Cr no. = 15–16 [Cr no. = 100Cr / (Cr + Al); cations per formula unit]. No significant difference was observed between crystal core and rim.

P-T conditions and evolution

Pressure was estimated following the method suggested by Köhler and Brey (1990), as the sample studied is a "normal" spinel peridotite, with Cr no. in spinel between 5–35. Two equations were utilized:

$$P\ (\text{kbar}) = (-T \cdot \ln D_{Ca} - 11982 + 3.61 \cdot T) / 56.2, \text{ for } T\ (\text{K}) \geq (1275.25 + 2.827 \cdot P) \quad (1)$$

or

$$P\ (\text{kbar}) = (-T \cdot \ln D_{Ca} - 5792 + 1.25 \cdot T) / 42.5, \text{ for } T\ (\text{K}) \leq (1275.25 + 2.827 \cdot P) \quad (2)$$

Moreover, taking into account the fact that the Ca exchange reaction between olivine and clinopyroxene is more dependent on temperature than on pressure, the first variable was estimated independently from the two-pyroxene thermometer (Brey and Köhler 1990), calibrated by these authors on the same experimental data as the olivine-clinopyroxene thermobarometer. A pressure of 15 kbar was assumed for this purpose, as the two-pyroxene thermometer depends slightly on pressure, which leads to a small error for the pressure domain of spinel lherzolites. The value for D_{Ca}^{ol-cpx} (= Ca^{ol} /Ca^{cpx}, where Ca^{ol} and Ca^{cpx} are the atomic proportions of Ca in the respective mineral formulae) was calculated from the EMPA data.

From the temperature estimated with the two-pyroxene thermometer, one of the two equations above was selected to estimate pressure. Once the pressure was estimated, the reverse procedure was followed to solve the temperature from Equation 1 or 2, assuming a pressure of 15 kbar. If the result did not agree with temperature calculated from the two-pyroxene thermometer, we assumed that either the two selected olivine-clinopyroxene points are not at equilibrium or that there was an analytical error, which is likely due to the SF effect. Thus, we validate the SF correction in this application and discuss the meaning of Ca profiles in olivine. We have applied this procedure first to uncorrected olivine analyses and then to the same data using the proposed SF correction procedure.

To assess the thermal evolution of xenolith sample CA.00.83, three profiles were measured in olivine crystals, from the rim toward the crystal core, until the distance from the interface was large enough to avoid the SF effect (Fig. 6). Special care was taken in selecting olivine areas without cracks. The shape of the olivine-clinopyroxene interface was assumed

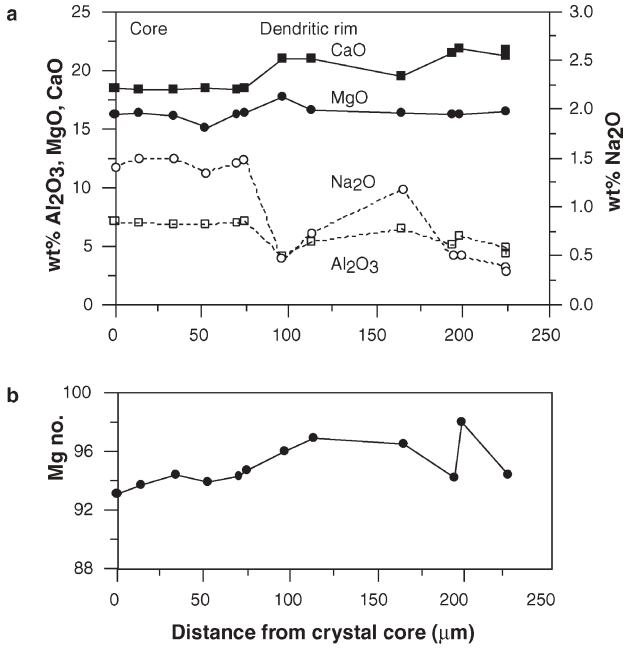

FIGURE 4. Compositional profile of a clinopyroxene crystal with a dendritic rim showing variations in wt% CaO, MgO, Al_2O_3, and Na_2O (**a**) and Mg no. (**b**).

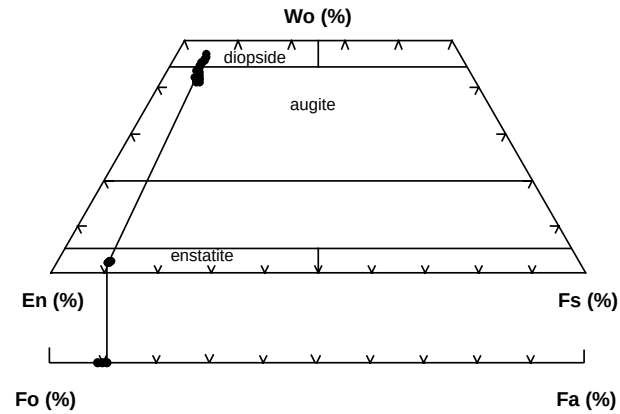

FIGURE 5. Quadrilateral plot for pyroxenes in sample CA.00.83. The range in Fo content for coexisting olivine is also illustrated.

to be planar but, as happens in natural samples, it was actually unknown. Profile 1 corresponds to an olivine crystal adjoining a clinopyroxene crystal without a dendritic rim, whereas the other profiles (2 and 3) adjoin clinopyroxene crystals with dendritic rims. As shown in Figure 6, there are no significant differences between the two types of profile: the Ca concentration seems to increase regularly at 40 μm from the crystal border, from 0.09 up to 0.18 wt%. However, after the SF correction, only profile 3 (Fig. 6c) clearly shows a slight increase in Ca at the border, from 0.08 to 0.13 wt%. The Ca-enriched rim is limited to 30 μm from the interface. The maximum contamination in Ca due to the SF effect is 0.06 wt%.

Temperatures estimated with the two-pyroxene thermometer decrease from the crystal core (1160 ± 4 °C) (2σ) to the crystal dendritic rim (1044 ± 35 °C) (Fig. 7). This finding seems to contradict a heating event as the cause of the clinopyroxene partial melting (Takahashi 1989; Tsuchiyama 1986; Köhler and Brey 1990; Shaw and Edgar 1997).

Maximum pressures estimated with Equations 1 and 2 are slightly higher for profile 1 in Figure 6 (the olivine adjoins a clinopyroxene crystal without a dendritic rim) than for profiles 2 and 3. For the first profile, the average pressure obtained is 19.5 ± 0.8 kbar (2σ) using uncorrected data and 20.9 ± 0.4 kbar, using data corrected for the SF effect (Fig. 7). Therefore, the SF correction leads to a higher pressure value with better precision. For this profile, no significant difference is observed between pressure estimations at the olivine crystal core and rim. Profiles 2 and 3 are more complex. The average pressure obtained for profile 2 is lower than for profile 1, using both corrected (17.0 ± 0.4 kbar) and uncorrected (14.6 ± 2.4 kbar) data, but higher pressure and improved precision are obtained when the SF correction is included. It should be pointed out that pressure decreases drastically from 16.5 to 2.5 kbar toward the olivine border when the SF correction is not included. This is not the case for profile 2 once the SF effect is corrected. However, for profile 3, the pressure decreases from 17.7 to 7.3 kbar toward the olivine rim, even after the SF correction.

The above-mentioned pressure data were estimated using the clinopyroxene core compositions. However, it is likely that for profiles 2 and 3, the olivine rim would be at equilibrium with the clinopyroxene dendritic rim and both would register later re-equilibration. Therefore, we have also estimated pressures by using compositions of the clinopyroxene dendritic rim and olivine data points at the border, until results using both corrected and uncorrected data match each other. In this case, the average pressure estimation for profile 2 is lower than for profile 1. Using corrected data, pressure values are found to be always higher and uncertainty lower (12.4 ± 0.9 kbar) than using uncorrected data (8.5 ± 1.5 kbar) (Fig. 7). For profile 3, resulting pressures using both corrected and uncorrected data were negative in most cases. For this reason, we infer that the clinopyroxene dendritic rim and olivine border are not at equilibrium. For this profile, we also estimated pressure by using a clinopyroxene composition close to the border, but outside the dendritic rim. Results are very similar to those obtained for profile 2: 9.0 ± 2.6 kbar using uncorrected data and 12.5 ± 1.6 kbar using data corrected for the SF effect.

Integrating all these results, we infer that the earlier pressure conditions registered by this xenolith are 21 kbar (olivine-clinopyroxene pair, the latter mineral without dendritic rim), followed by 17 kbar (olivine core-clinopyroxene core, clinopyroxene with dendritic rim), and then 12 kbar (olivine rim-clinopyroxene dendritic rim). This pressure drop is illustrated in Figure 7 together with temperatures estimated with the two-pyroxene thermometer. A typical adiabatic decompression path is observed (its lowest pressure is inferred from the few consistent pressure values obtained using the clinopyroxene dendritic rim from profile 3). The *P-T* path obtained from uncorrected EMPA data is also shown. It should be pointed out that the highest pressure estimated using corrected data is closer

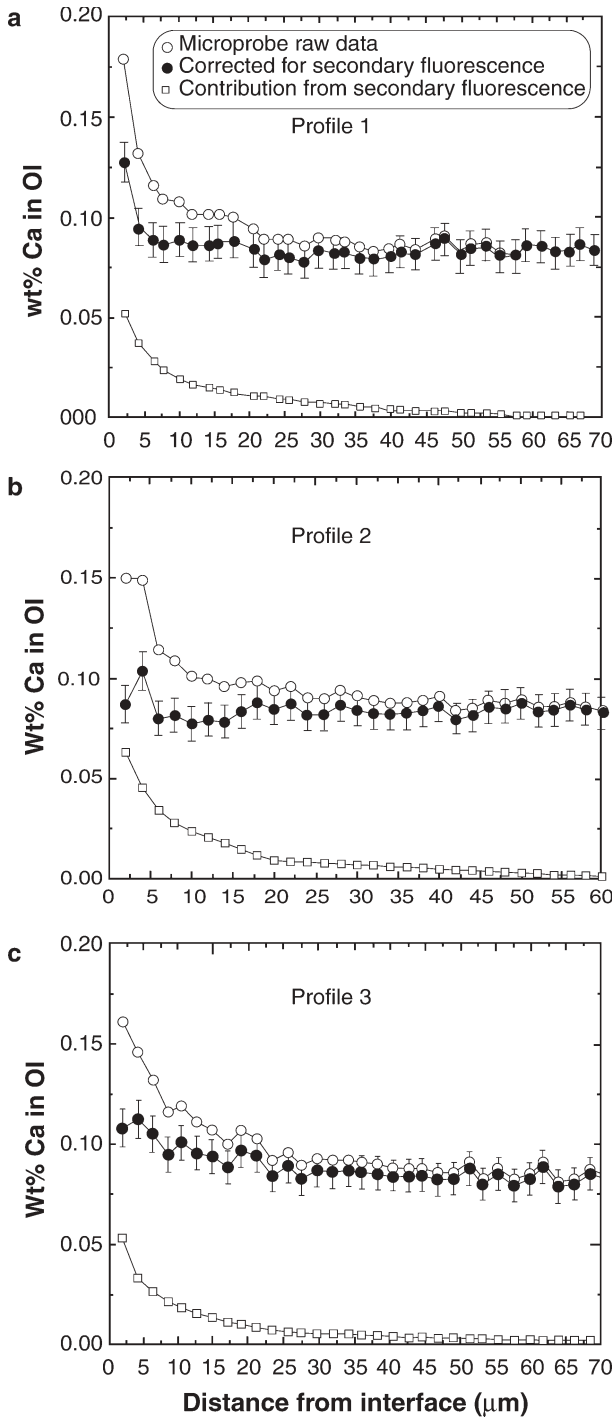

FIGURE 6. Profiles showing wt% CaO in olivine crystals adjoining clinopyroxene crystals without (**a**) and with (**b** and **c**) dendritic rims. Both corrected and uncorrected concentrations are shown together with contributions from secondary fluorescence. Statistical error (2σ) for corrected data is indicated.

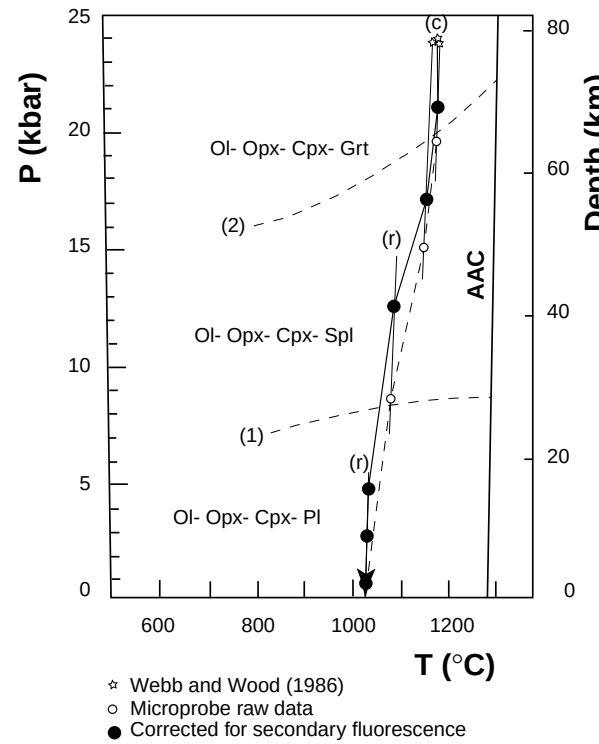

FIGURE 7. *P-T* conditions and evolution for sample CA.00.83 using corrected and uncorrected data for the olivine-clinopyroxene barometer (Köhler and Brey 1990). The *P-T* path from the former is represented by a solid line and from the latter by a dashed line. Pressures are also estimated after Webb and Wood (1986). Temperatures correspond to the two-pyroxene thermometer (Brey and Köhler 1990). AAC stands for the adiabatic ascent curve for normal temperature asthenosphere (McKenzie and Bickle 1989). (1) and (2) are the reaction boundaries between plagioclase lherzolites and spinel lherzolites (Gasparik 1987), and between spinel lherzolites and garnet lherzolites (O'Neill 1981; Klemme and O'Neill 2000), respectively. c and r stand for crystal core and rim respectively. See text for further explanation.

to the maximum pressure of spinel peridotites calculated after the method of Webb and Wood (1986), whereas it is much lower with uncorrected data. Although the type of path determinated from uncorrected data is similar, it is always shifted to slightly higher temperatures. From the adiabatic ascent curve (AAC in Fig. 7) for normal temperature asthenosphere (McKenzie and Bickle 1989), we also deduce that this xenolith was extracted from ca. 80 km depth, which indicates a minimum lithosphere thickness in the area at the time of the volcanic activity.

When Equations 1 or 2 are used as geothermometers, assuming P = 15 kbar, we found that temperature values agree much better with the ones obtained from the two-pyroxene thermometer if the SF correction is performed. Figure 8 shows the deviation (in %) of the temperature estimated from the olivine-clinopyroxene thermometer with respect to the value determined with the two-pyroxene thermometer, defined as follows:

$$\text{Deviation} = 100 \cdot (\text{TKB} - \text{TBK})/\text{TBK} \quad (3)$$

where TKB stands for the olivine-clinopyroxene temperature (Köhler and Brey 1990), and TBK is the two-pyroxene temperature (Brey and Köhler 1990).

We can see that for profile 1 (Fig. 8a), the deviation is relatively constant (–2%) when using corrected data. On the other hand, when uncorrected data are used, the deviation increases slightly toward the border and reaches a maximum of +3%. This finding apparently suggests a heating event, which would contradict the two-pyroxene temperatures. Figures 8b and 8c show a similar trend for profile 2: the deviation of corrected data is ±2%, but for uncorrected data, it amounts to +11% at the olivine rim. Therefore, for profiles 1 and 2, if EMPA analyses for Ca are not corrected for the effect of SF, the olivine-clinopyroxene thermometer indicates an apparent heating event. The accuracy obtained for profile 3 is not so well defined, as shown in Figures 8d, 8e, and 8f. Deviation of both corrected and uncorrected data is better at the core (–3%) than at the rim (+12% and +18% for corrected and uncorrected data, respectively). A likely explanation would be that there is disequilib-

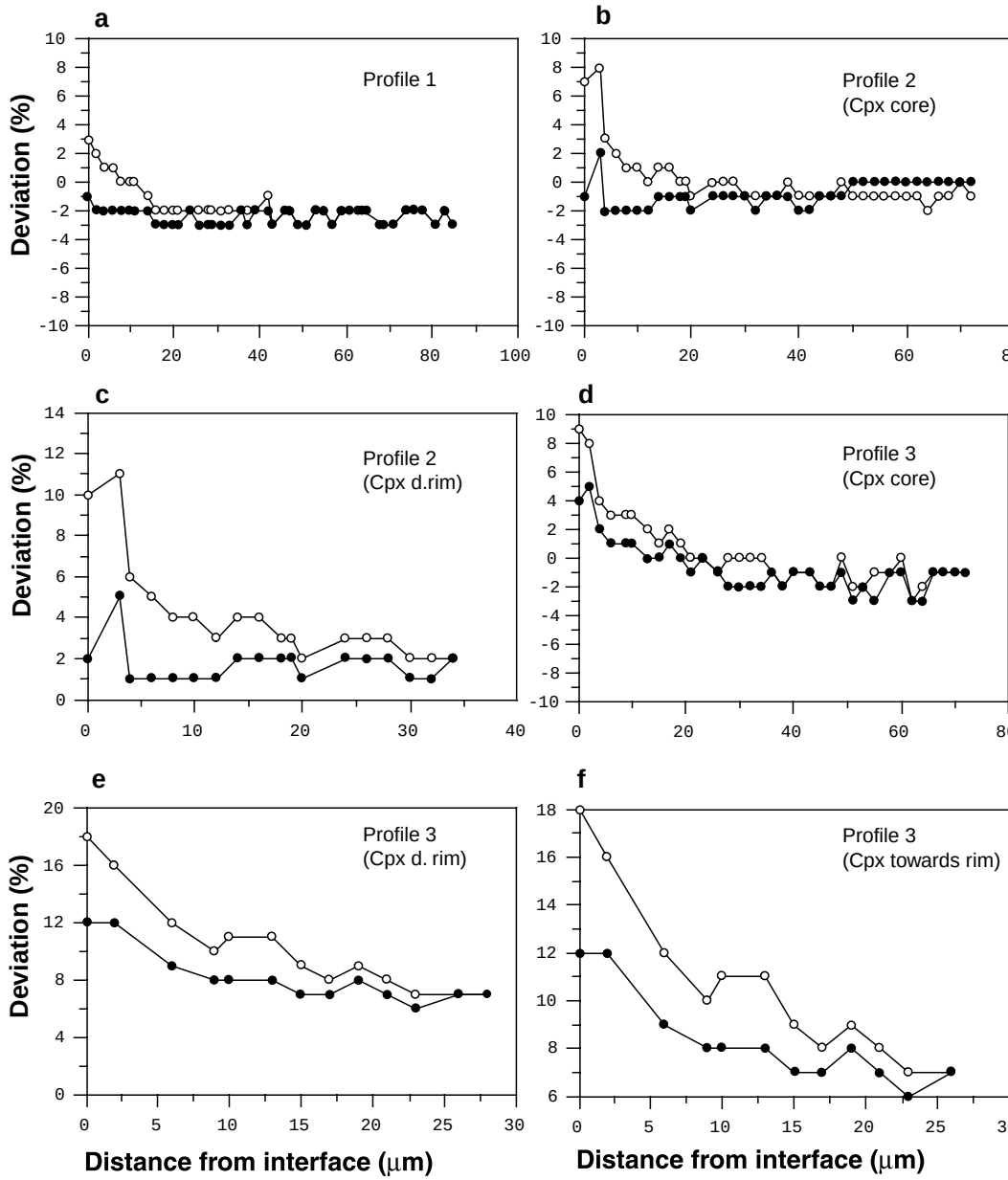

FIGURE 8. (a–f) Comparison between the two-pyroxene temperature and the Ol-Cpx temperature expressed as deviation vs. Distance from interface in the three olivine profiles. Data for raw microprobe data and SF corrected data are illustrated. Symbols as in Figure 7. Clinopyroxene crystal core and rim compositions are considered. See text for further discussion.

rium between the two minerals, as is further supported by the inconsistent negative pressure estimations. Thus, the partial melting of clinopyroxene and the increase of the Ca concentration at the rim of some olivine crystals could be due to adiabatic decompression of the spinel lherzolite (Fig. 7) rather than to heating by the host lava.

ACKNOWLEDGMENTS

Financial support for this study was obtained from the CICYT project PB97-0198-C02-01. L. McAllister is thanked for the revision of the English spelling and S.J.B. Reed for helpful comments on an earlier version of the manuscript. C. Merlet is thanked for helpful discussions.

REFERENCES CITED

Acosta, E., Llovet, X., Coleoni, E., Riveros, J.A., and Salvat, F. (1998) Monte Carlo simulation of X-ray emission by kilovolt electron bombardment. Journal of Applied Physics, 83, 6038–6049.

Adams, G.E. and Bishop, F.C. (1986) The olivine-clinopyroxene geobarometer: experimental results in the CaO-FeO-MgO-SiO_2 system. Contributions to Mineralogy and Petrology, 94, 230–237.

Araña, V., Aparicio, A., Martín Escorza, C., García Cacho, L., Ortiz, R., Vaquer, R., Barberi, F., Ferrara, G., Albert, J., and Gassiot, X. (1983) El volcanismo neógeno-cuaternario de Catalunya: caracteres estructurales, petrológicos y geoquímicos. Acta Geológica Hispánica, 18, 1–17.

Baró, J., Sempau, J., Fernández-Varea, J.M., and Salvat, F. (1995) PENELOPE: an algorithm for Monte Carlo simulation of the penetration and energy loss of electrons and positrons in matter. Nuclear Instruments and Methods in Physics Research B, 100, 31–46.

Bastin, G.F., van Loo, F.J.J., Vosters, P.J.C., and Vrolijk, J.W.G.A. (1983) A correction procedure for characteristic fluorescence encountered in microprobe analysis near phase boundaries. Scanning, 5, 172–183.

Brey, G.P. and Köhler, T. (1990) Geothermobarometry in Four-phase Lherzolites II. New Thermobarometry, and Practical Assessment of Existing Thermo-barometers. Journal of Petrology, 31, 1353–1378.

Cebriá, J.M., López- Ruiz, J., Doblas, M., Oyarzun, R., Hertogen, J., and Benito, R. (2000) Geochemistry of the Quaternary alkali basalts of Garrotxa (NE Volcanic Province, Spain): a case of double enrichment of the mantle lithosphere. Journal of Volcanology and Geothermal Research, 102, 217–235.

Dalton, J.A. and Lane, S.J. (1996) Electron microprobe analysis of Ca in olivine close to grain boundaries: the problem of secondary X- ray fluorescence. American Mineralogist, 81, 194–201.

Douckhan, N., Douckhan, J-C., Ingrin, J., Jaoul, O., and Raterron, P. (1993) Early partial melting in pyroxenes. American Mineralogist, 78, 1246–1256.

Feenstra, A. and Engi, M. (1998) An experimental study of the Fe-Mn exchange between garnet and ilmenite. Contributions to Mineralogy and Petrology, 131, 379–392.

Gasparik, T. (1987) Orthopyroxene thermobarometry in simple and complex systems. Contribution to Mineralogy and Petrology, 96, 357–370.

Jurewicz, A.J.G. and Watson, E.B. (1988) Cations in olivine, Part 1: Calcium partitioning and calcium- magnesium distribution between olivines and coexisting melts, with petrologic applications. Contributions to Mineralogy and Petrology, 99, 176–185.

Klemme, S. and O'Neill, H. StC. (2000) The near-solidus transition from garnet lherzolite to spinel lherzolite. Contributions to Mineralogy and Petrology, 138, 237–248.

Köhler, T.P. and Brey, G.P. (1990) Calcium exchange between olivine and clinopyroxene calibrated as geothermobarometer for natural peridotites from 2 to 60 kb with applications. Geochimica et Cosmochimica Acta, 54, 2375–2388.

Kretz, R. (1983) Symbols for rock forming minerals. American Mineralogist, 68, 277–279.

Llovet, X., Valovirta, E., and Heikinheimo, E., (2000) Monte Carlo simulation of secondary fluorescence in small particles and at phase boundaries. Mikrochimica Acta, 132, 205–212.

López Ruiz, J. and Rodríguez Badiola, E. (1983) La región volcánica Mio-Pleistocena del NE de España. Estudios Geológicos, 41, 105–126.

Maaskant, P. and Kaper, H. (1991) Fluorescence effects at phase boundaries: petrological implications for Fe-Ti oxides. Mineralogical Magazine, 55, 277–279.

Martí, J., Mitjavila, J., Roca, E., and Aparicio, A. (1992) Cenozoic magmatism of the Valencia trough (western Mediterranean): relationship between structural evolution and volcanism. Tectonophysics, 203, 145–165.

McKenzie, D. and Bickle, M.J. (1989) The Volume and Composition of Melt Generated by Extension of the Lithosphere. Journal of Petrology, 29, 625–679.

Morimoto, N., Fabries, J., Ferguson, A.K., Ginzburg, I.V., Ross, M., Seifert, F.A., Zussman, J., Aoki, K., and Gottardi, G. (1988) Nomenclature of Pyroxenes. Mineralogy and Petrology, 39, 55–76.

Myklebust, R.L. and Newbury, D.E. (1994) Monte Carlo modeling of secondary X-ray fluorescence across phase boundaries in electron probe microanalysis. Scanning, 17, 235–242.

Nixon, H., Ed. (1987) Mantle Xenoliths, 844 p. John Wiley and Sons, Chichester.

O'Neill, H. StC. (1981) The transition between spinel lherzolite and garnet lherzolite, and its use as a geobarometer. Contributions to Mineralogy and Petrology, 77, 185–194.

Pouchou, J. (1996) Use of soft X-rays in microanalysis. Mikrochimica Acta [Supplement] 13, 39–60.

Pouchou, J.L. and Pichoir, F. (1984) A new model for quantitative analysis. Application to the analysis of homogeneous samples. La recherche aérospatiale, 5, 47–65.

Reed, S.J.B (1993) Electron microprobe analysis. Cambridge University Press, Cambridge.

Robinson, P. (1982) The composition space of Terrestrial Pyroxenes-Internal and External Limits. In C.T. Prewitt, Ed., Pyroxenes, 7, p 419– 494, Mineralogical Society of America, Reviews in Mineralogy, Washington D.C.

Sempau, J., Acosta, E., Baró, J., Fernández-Varea, J.M., and Salvat, F. (1997) An algorithm for Monte Carlo simulation of coupled electron-photon transport. Nuclear Instruments and Methods in Physics Research, B, 132, 377–390.

Shaw, C.S.J. and Edgar, A.D. (1997) Post-entrainment mineral-melt reactions in spinel peridotite xenoliths from Inver, Donegal, Ireland. Geological Magazine, 134, 771–779.

Takahashi, E. (1989) Thermal history of lherzolite xenoliths-I. Petrology of lherzolite xenoliths from the Ichinomegata crater, Oga peninsula, northeast Japan. Geochimica et Cosmochimica Acta, 44, 1643–1658.

Tournon, J. (1968) Le Volcanisme de la Province de Gérone (Espagne). Etudes de basaltes quaternaires et de leurs enclaves. Thèsis p. 1–128, Paris.

Tsuchiyama, A. (1986) Melting and dissolution kinetics: application to partial melting and dissolution of xenoliths. Journal of Geophysical Research, 91, 9395–9406.

Valovirta, E., Erlach, S., Llovet, X., and Heikinheimo, E. (2001) EPMA of metal-metal diffusion couples at high temperature. Influence of secondary fluorescence effects. Proceedings EMAS 2001, p. 382, Tampere, Finland.

Webb, S.A.C. and Wood, B.J. (1986) Spinel- pyroxene- garnet relationships and their dependence on Cr/Al ratio. Contributions to Mineralogy and Petrology, 92, 471–480.

Werling, F. and Althe, R. (1997) Thermal evolution of the lithosphere beneath the French Massif Central as deduced from geothermobarometry on mantle xenoliths. Tectonophysics, 275, 119–141.

Wilson, M. and Downes, H. (1990) Tertiary- Quaternary Extension Related Alkaline Magmatism in Western and Central Europe. Journal of Petrology, 32, 811–849.

Witt-Eickschen, G. (1993) Upper mantle xenoliths from alkali basalts of the Vogelsberg, Germany: implications for mantle upwelling and metasomatism. European Journal of Mineralogy, 5, 361–376.

Witt-Eickschen, G. and Kramm, U. (1997) Mantle Upwelling and Metasomatism beneath Central Europe: Geochemical and Isotopic Constraints from Mantle Xenoliths from the Rhön (Germany). Journal of Petrology, 38, 479–493.

MANUSCRIPT RECEIVED NOVEMBER 6, 2001
MANUSCRIPT ACCEPTED JULY 17, 2002
MANUSCRIPT HANDLED BY JOHN C. SCHUMACHER